



# Large-scale commodity agriculture exacerbates the climatic impacts of Amazonian deforestation

Eduardo Eiji Maeda<sup>a,1</sup>, Temesgen Alemayehu Abera<sup>a,b</sup>, Mika Siljander<sup>a</sup>, Luiz E. O. C. Aragão<sup>c,d</sup>, Yhasmin Mendes de Moura<sup>e</sup>, and Janne Heiskanen<sup>a,b</sup>

<sup>a</sup>Department of Geosciences and Geography, University of Helsinki, FI-00014 Helsinki, Finland; <sup>b</sup>Institute for Atmospheric and Earth System Research, Faculty of Science, University of Helsinki, FI-00014 Helsinki, Finland; <sup>c</sup>Earth Observation and Geoinformatics Division, National Institute for Space Research, 12227-010 São José dos Campos, SP, Brazil; <sup>d</sup>College of Life and Environmental Sciences, University of Exeter, EX4 4RJ Exeter, United Kingdom; and <sup>e</sup>Newton International Fellow, Centre for Landscape and Climate Research, School of Geography, Geology and Environment, University of Leicester, LE1 7RH Leicester, United Kingdom

Edited by B. L. Turner, Arizona State University, Tempe, AZ, and approved December 29, 2020 (received for review November 20, 2020)

In the Amazon rainforest, land use following deforestation is diverse and dynamic. Mounting evidence indicates that the climatic impacts of forest loss can also vary considerably, depending on specific features of the affected areas. The size of the deforested patches, for instance, was shown to modulate the characteristics of local climatic impacts. Nonetheless, the influence of different types of land use and management strategies on the magnitude of local climatic changes remains uncertain. Here, we evaluated the impacts of large-scale commodity farming and rural settlements on surface temperature, rainfall patterns, and energy fluxes. Our results reveal that changes in land-atmosphere coupling are induced not only by deforestation size but also, by land use type and management patterns inside the deforested areas. We provide evidence that, in comparison with rural settlements, deforestation caused by large-scale commodity agriculture is more likely to reduce convective rainfall and increase land surface temperature. We demonstrate that these differences are mainly caused by a more intensive management of the land, resulting in significantly lower vegetation cover throughout the year, which reduces latent heat flux. Our findings indicate an urgent need for alternative agricultural practices, as well as forest restoration, for maintaining ecosystem processes and mitigating change in the local climates across the Amazon basin.

land use | deforestation | agricultural expansion | Amazon forest | regional climate

During the past 50 y, ~20% of the Amazon forest has been lost to deforestation (1, 2). These changes in the land surface have affected the functioning of ecosystems and the climate in ways we are only starting to understand. Deforestation size, for instance, is a potential factor defining the magnitude and characteristics of changes in local climate associated with forest loss (3, 4). There is also evidence that the different land uses that follow deforestation can regulate the magnitude of changes in surface energy balance and water cycle (5). Historically, there has been large variation in the characteristics and causes of deforestation (1, 6–9). In the area known as the “arc of deforestation,” two major processes have contributed to forest loss: government-supported rural settlements and expansion of market-focused large-scale agriculture (hereinafter referred to as “commodity agriculture”) (10, 11). Deforestation caused by these two types of farming systems has distinct characteristics, and each can have several variants.

Rural settlements are generally associated with government colonization projects, migratory flow incentives, and the construction of new roads (7). In areas dominated by rural settlements, small properties with plots ranging from 25 to 100 ha are predominant (8, 9, 12). However, medium-sized properties ranging from 250 to 1,000 ha and farms larger than 1,000 ha may also occur. Activities inside these areas are characterized by livestock production (extensive pastures), small-scale crop production, and family farming (13). The establishment of small farms along main

highways and secondary roads results in the well-known “fish bone” deforestation pattern.

Forest areas taken by large-scale commodity agriculture represent a more recent stage of occupation, usually associated with spontaneous and economical migration but also, with changes in land use policies and market conditions (14). Agricultural activities aimed at commodity crop plantation are in general productive and often technologically advanced. The most common commodity crops in the Amazon region are soybean, maize, sorghum, and cotton. Nonetheless, forests are typically not converted directly into croplands, with pastures often used as a transitory land use. Permanent mid- to large-scale cattle ranching also occurs, although many of these areas are being rapidly converted into croplands (6, 14–16). Farm sizes can reach several thousand hectares. Properties are, therefore, bigger and more isolated, in comparison with rural settlements (13).

Given the different characteristics of commodity agriculture and rural settlements, the spatiotemporal patterns of land cover biophysical properties can also differ considerably. In general, commodity crops cultivation involves an intensive use of the land, sometimes with two or more harvests per year (17). Hence, rapid changes in the vegetation cover, albedo, and evapotranspiration (ET) can occur (5, 18). On the other hand, in areas where small-scale pastures and agriculture are prevalent, the biophysical properties of the land surface are expected to vary less, given the

## Significance

The southern Amazon is one of the fastest changing places on Earth. Deforestation is giving place to a dynamic and diverse landscape, comprising small-scale farmers and large-scale commercial agriculture with differing land uses. Understanding how these different land uses affect ecosystems and local climates is essential for promoting strategies to mitigate environmental changes. Here, we show that large-scale commercial agriculture leads to a higher increase in surface temperature, in comparison with small-scale farms. We also found evidence that changes in land surface attributes over large commercial farms lead to a more prominent reduction in rainfall volumes. Our results provide compelling arguments indicating that changes in farming practices are needed to guaranty a sustainable future in the Amazon region.

Author contributions: E.E.M. designed research; E.E.M., T.A.A., and Y.M.d.M. performed research; E.E.M., T.A.A., M.S., L.E.O.C.A., Y.M.d.M., and J.H. analyzed data; L.E.O.C.A. and J.H. edited the manuscript and interpreted results; and E.E.M. wrote the paper.

The authors declare no competing interest.

This article is a PNAS Direct Submission.

Published under the PNAS license.

<sup>1</sup>To whom correspondence may be addressed. Email: eduardo.maeda@helsinki.fi.

This article contains supporting information online at <https://www.pnas.org/lookup/suppl/doi:10.1073/pnas.2023787118/-DCSupplemental>.

Published February 8, 2021.

less intensive use of the land (e.g., associated with family farming and agroforestry). Furthermore, modeling studies suggest that the type of vegetation involved in land cover conversions is important in determining the sign of the land change impacts (19). However, empirical studies are crucially needed to better understand how different land uses across the Amazon region affect the local and regional climate.

Tropical deforestation has deep impacts on biophysical processes (1, 20–22), contributing to amplifying diurnal temperature variability ( $1.95 \pm 0.08$  °C) as well as increasing mean air temperature ( $\sim 1$  °C) (23). The causes of increase in temperature are dominated by nonradiative mechanisms, in particular a decrease in latent heat flux (LE) (24). The cooling effects of albedo increase due to deforestation are in most cases outweighed by the warming effects of decreasing ET, leading to net warming (23–25).

The impacts of Amazon deforestation on rainfall patterns are not yet fully understood (4). In the initial phases of deforestation, vegetation loss was shown to increase regional cloudiness and precipitation (3). In comparison with deforested areas, the greater humidity over forests leads to more convective available potential energy, which makes the atmospheric boundary layer more unstable (26). Conversely, small deforestation patches showed more active shallow convection, explaining the higher frequency of shallow clouds over deforested areas (26). However, it is unclear how these mechanisms change as deforested areas increase and land cover becomes more uniform. One hypothesis is that convective lifting mechanisms will lose force, and shallow clouds over deforested areas will no longer be favored. Modeling studies indicate that this shift is already happening in some parts of the Amazon, where deforestation has reached a point in which thermally dominated regime has declined, leading to a more dynamically driven hydroclimatic regime (27). A dynamically driven regime becomes dominant when differences in surface roughness between forest and forest clearings start to play a larger role in the atmospheric response, in comparison with the differences in the surface energy partitioning (28).

As observational and modeling studies indicate that land use and management can play an important role in the climate system, overlooking these landscape heterogeneities can hinder an adequate response to the threats posed by human activities (29). Clarifying the climatic impacts of different land uses in the Amazon is crucial to foster informed plans for sustainable land management, in particular those aiming at strategies for climate change mitigation, maintenance of ecological functioning, and guarantying provision of essential ecosystem services. Here, we hypothesize that forest conversion to large-scale commodity agriculture is more detrimental to local climate than conversion to rural settlements. To test this hypothesis, we first evaluated whether or not land uses associated with commodity agriculture and rural settlements lead to quantitatively distinguishable land cover spatiotemporal patterns in regions with similar deforestation rates (1985 to 2018) and total deforested area in 2018. Next, we collected empirical evidence on how forest clearing associated with these two causes has affected local rainfall, surface temperature, and LE.

## Results

**Landscape Patterns across Rural Settlements and Commodity Agriculture Areas.** Our analysis focused on four areas ( $\sim 110 \times 110$  km each) in the Amazon basin (Fig. 1). The criteria and procedures used to select the study areas are described in *Study Areas*. Two areas were located in the arc of deforestation (marked as cells A and C in Fig. 1). Cell A was located in the state of Rondônia, over an area dominated by a fish bone deforestation pattern formed by small farms distributed along main highways and secondary roads. Cell C was located in the north of Mato Grosso State, over an area where large-scale commodity farms are prevalent. The mean size of consolidated area per property in cell A was 52 ha, while in cell C, the mean size of consolidated area

per property was 374 ha (*SI Appendix, Fig. S2*). In addition, two areas with similar size but not affected by deforestation were used as reference sites (marked as cells B and D in Fig. 1).

In both areas affected by land changes (cells A and C), deforested area in the beginning of the 1980s accounted for less than 10% of the total area (Fig. 1A). A step increase in forest loss occurred between 1990 and 2005, after which the total area deforested stabilized at  $\sim 40\%$ . Despite similar amounts of total area deforested, the spatial patterns of the two regions could be distinguished visually and quantitatively (Fig. 1). Until the late 1990s, landscape in both regions displayed similar core area (i.e., the total area of patches that have only neighboring patches from the same class). After the year 2000, the core area of forests in the area dominated by fish bone deforestation (“rural settlements”) increased at a higher rate in comparison with areas allocated for commodity agriculture. The shape complexity, expressed by the shape index (i.e., the ratio between the perimeter of the patch and the hypothetical minimum perimeter of the patch), was consistently higher ( $\sim 10\%$ ) in the commodity agriculture areas in comparison with the rural settlements.

Land use in rural settlement areas (cell A) was largely dominated by pastures throughout the entire study period, with only small areas designated to croplands ( $<1\%$ ) (Fig. 1 and *SI Appendix, Fig. S3*). Other activities such as family farming and agroforestry, although present, are likely masked due to the small scale of these activities. Given that these land use types are not specifically accounted for in the dataset used for this analysis, they are often misclassified as pastures. In the commodity agriculture area (cell C), a shift in land use patterns took place after the year 2000, with a steady increase in areas designated to croplands, reaching  $\sim 25\%$  of the entire area in 2018. The increase in croplands was accompanied by a decrease in areas destined to pastures, which decrease from 22% in 2005 to 13% in 2018 (Fig. 1 and *SI Appendix, Fig. S3*).

We further demonstrate that land cover temporal patterns differ between the two sites. Vegetation cover over deforested areas was assessed using satellite-derived enhanced vegetation index (EVI). Areas of commodity agriculture had consistently and significantly (unpaired Welsch *t* test,  $P < 0.01$ ) lower vegetation cover between May (day of year [DOY] = 120) and November (DOY = 305) (Fig. 2A). Between December and February, both areas had similar EVI values, indicating a comparable vegetation cover during this period. We also analyzed differences in the vegetation cover of dominant land use types in our study areas. In September, when vegetation cover was shown to be the lowest, croplands had  $\sim 20\%$  lower EVI than pastures inside the same region (i.e., cell C, mid- to large-scale cattle ranching) and 30% lower than pastures located in the rural settlement area (cell A).

**Changes in Rainfall Patterns.** Changes in the seasonal patterns of rainfall were evaluated based on the average of two periods: from 1998 to 2005 and from 2005 to 2014 (Fig. 3), thus comprising the entire time series of the TRMM (Tropical Rainfall Measuring Mission) precipitation radar (PR). These time intervals allowed the assessment of rainfall patterns from a period when the deforestation process was only beginning to a period when forest loss was relatively stable. The average forest cover percentage in cells A and C was at 83% from 1998 to 2005, and it declined to 57% from 2005 to 2014.

We observed decreasing rainfall rates in the commodity agriculture site (Figs. 3 and 4). The reduction occurred mostly during months with average monthly rainfall above 200 mm  $\text{mo}^{-1}$  (i.e., the period between October and March, hereinafter referred to as “wet season”), being particularly evident in February, March, October, and November. The decrease was shown to be mainly caused by a reduction in convective rainfall, while changes in stratiform rain were less evident (Fig. 3). When considering the annual mean, we observed significant differences in the mean

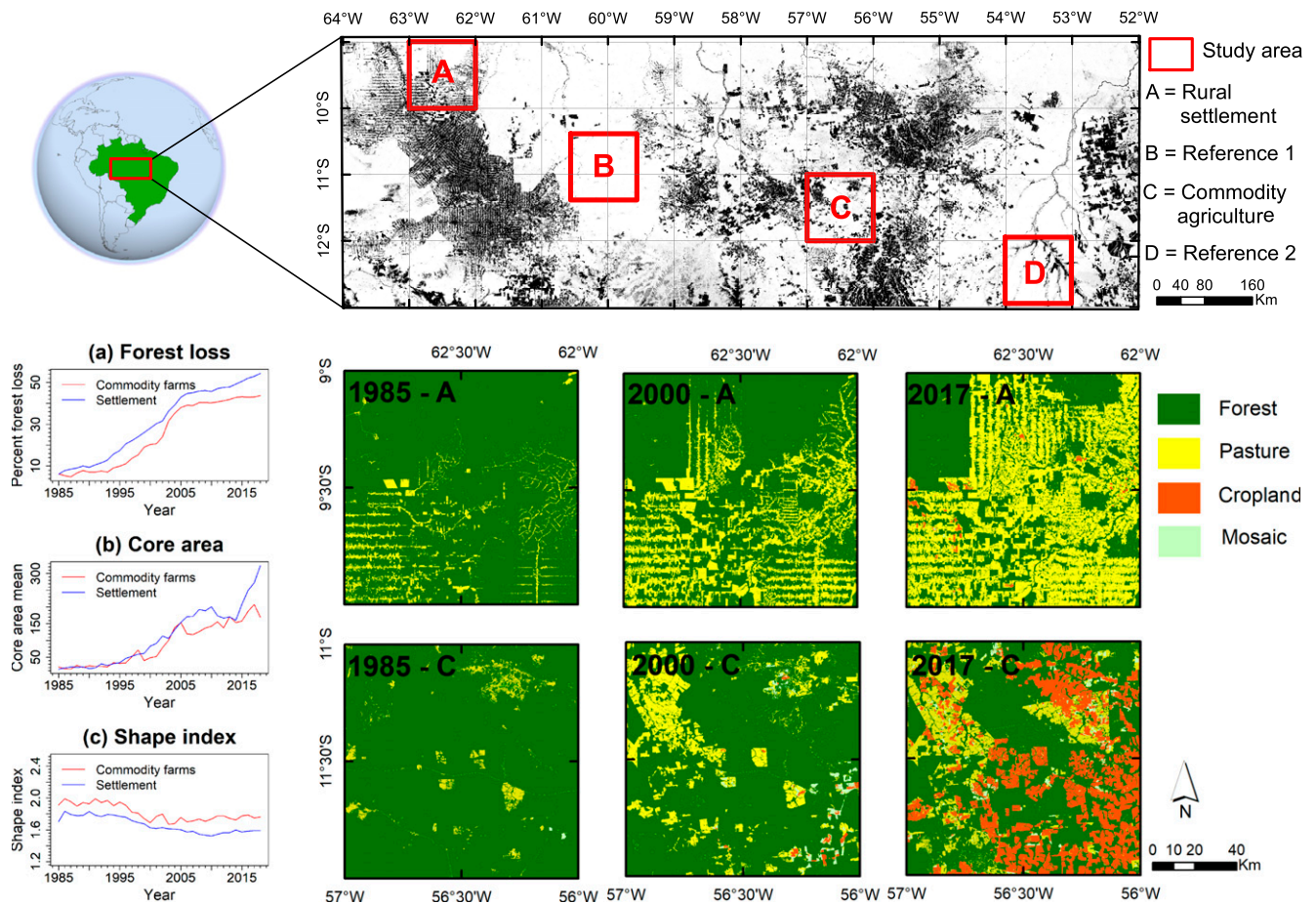


**Fig. 1.** Geographical locations of the study areas, each consisting of  $1^\circ \times 1^\circ$  cells, where cell A is dominated by rural settlements and cell C is dominated by large-scale commodity agriculture. Cells B and D were used as reference, as there has been no substantial forest loss in these areas during the study period. (A) Total forest loss, (B) mean core area of deforested areas, and (C) the mean shape index of deforested areas.

total and convective rain ( $P = 0.016$  and  $P = 0.009$ , respectively, based on a Welsch  $t$  test), while differences in the mean annual stratiform rain were not significant ( $P = 0.279$ ). A Mann–Kendall (M-K) trend test indicated a strong and consistent decreasing trend in convective rainfall ( $P = 0.006$ ) during the wet season between 1998 and 2014, while the stratiform rainfall trend during the same period had a lower magnitude ( $P = 0.012$ ) (Fig. 4). There were no significant trends in rainfall during the dry season (April to September) in the commodity agriculture site (Fig. 4).

In the rural settlements site, there were no clear changes in the seasonal patterns of rainfall between the two periods (Fig. 3). Annual mean values were also not statistically different (based on a paired Welsch  $t$  test). This result was confirmed by the M-K test, which did not indicate significant trends in convective or stratiform rainfall, independent of the season (Fig. 4).

To discard the influence of large-scale climatic signals in these results, we conducted the same analysis in two reference areas (i.e., cell B located between cells A and C in the northwest part

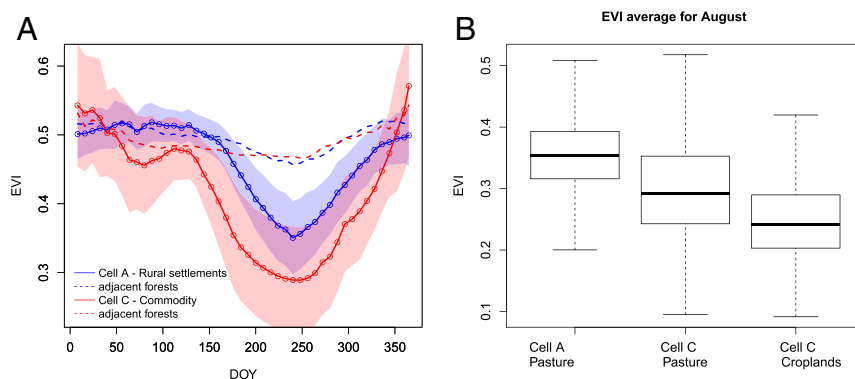


**Fig. 2.** (A) Seasonal variability in vegetation cover inside deforested areas (solid lines) and in adjacent forests (dashed lines) measured using the EVI. The adjacent forests represent intact forests located inside the same  $1^\circ \times 1^\circ$  cell. Average values were calculated using data from 2001 to 2018. Shaded areas represent means  $\pm$  SD. (B) August average EVI values for dominant land use classes inside each cell.

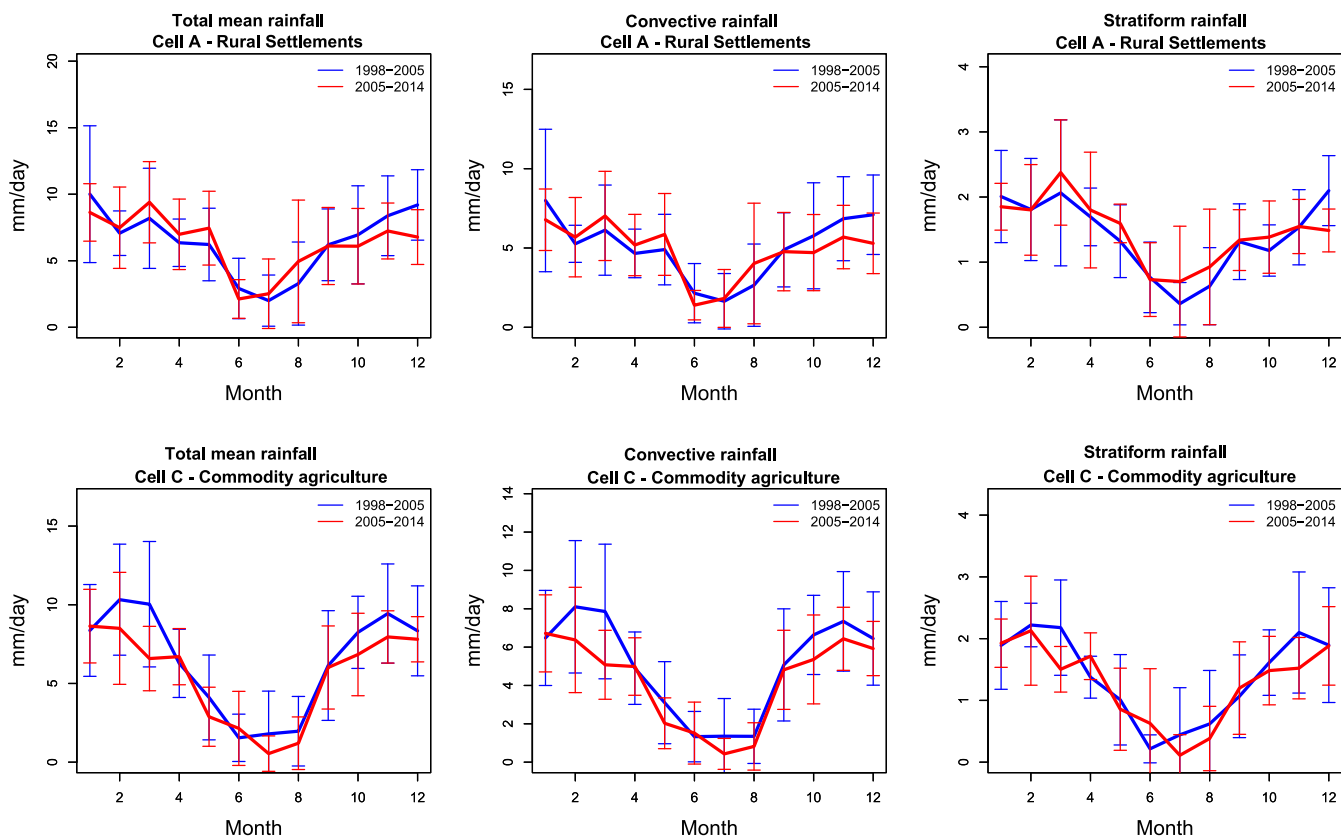


**Fig. 3.** Mean seasonal patterns of rainfall between 1998 and 2005 (blue lines; average forest cover = 83%) and between 2005 and 2014 (red lines; average forest cover = 57%).

of Mato Grosso State and cell D located inside the Xingu National Park—both areas showed no forest loss during the same period of time) (Fig. 1 and *SI Appendix*, Figs. S1, S4, and S5). The results confirmed that significant trends were not observed in the regions unaffected by deforestation.

**Changes in Land Surface Temperature and LE.** Changes in land surface temperature (LST), LE, and ET caused by forest loss were assessed using a space-for-time (SFT) substitution approach (30, 31). The basic assumption in the SFT substitution is that spatial and temporal variations are equivalent (30). Hence, observations over deforested areas were compared with those obtained over adjacent forests. We observed that both sites showed significant differences in LST between forested and deforested areas ( $P < 0.01$ ) (Fig. 5). These changes were present during all seasons of the year, although differences in the dry season had higher magnitude. Forest loss associated with rural settlements caused an average LST increase of 1.05 °C during the wet seasons and 1.25 °C during the dry seasons (Fig. 5A). The maximum average warming in rural settlement areas was observed in August (1.85 °C). In areas of commodity agriculture, warmings of 1.57 °C and 2.11 °C were observed in the wet and dry seasons, respectively. The maximum difference was also observed in August (3.06 °C). When untangling these results by land use type, we observed that, in August, croplands were on average ~1 °C warmer than pastures (Fig. 5). Both pastures in cell A and cell C showed similar mean temperatures for the same period (33.8 °C and 33.2 °C, respectively).

Changes in LE caused by forest loss were evident in both sites (Fig. 6). The magnitude and seasonal patterns of the changes were, however, more pronounced in deforested areas caused by commodity agriculture. In rural settlement areas, the decline of

LE (in relation to adjacent forests) was observed from June (DOY ~ 150) to the end of October (DOY ~ 300). In commodity agriculture areas, the decline occurred from May (DOY ~ 125) to mid-November (DOY ~ 325; i.e., ~50 d longer than the rural settlements area). In both areas, the strongest reduction in LE was observed around August to September. During this period, the LE decline in commodity agriculture areas was approximately two times larger than in fish bone areas (Fig. 6). During August, croplands had 39% lower LE than pastures located in the same region (cell C) and 60% lower LE than pastures located in rural settlement areas (cell A).

Changes in ET followed the same pattern (*SI Appendix*, Fig. S7A). In commodity agriculture areas, the lowest ET values were around 1.2 mm d<sup>-1</sup> (compared with 3 to 4 mm d<sup>-1</sup> in adjacent forests), while the minimum ET in fish bone areas reached ~2.4 mm d<sup>-1</sup>. The contribution of transpiration to total ET [ $T/(E + T)$ ] was consistently lower in commodity agriculture areas, in comparison with rural settlements (*SI Appendix*, Figs. S7 B–D), confirming the key role of vegetation cover on the stronger reduction of LE and ET in commodity agriculture areas. During August to September, when the strongest reduction in LE was observed,  $T/(E + T)$  was ~60% in commodity agriculture areas and 75% in rural settlements (*SI Appendix*, Fig. S7B).

Contrasting differences were also observed in the rainy season, particularly from January to May (Fig. 6 and *SI Appendix*, Fig. S7). During this period, rural settlement areas showed similar or higher LE and ET in comparison with adjacent forest areas. On the other hand, in commodity agriculture areas, LE and ET values were lower than in the original land cover, in particular between February and April (i.e., same period when a reduction in convective rainfall was observed). This result is again explained by a lower contribution of  $T$  to total ET, which was as

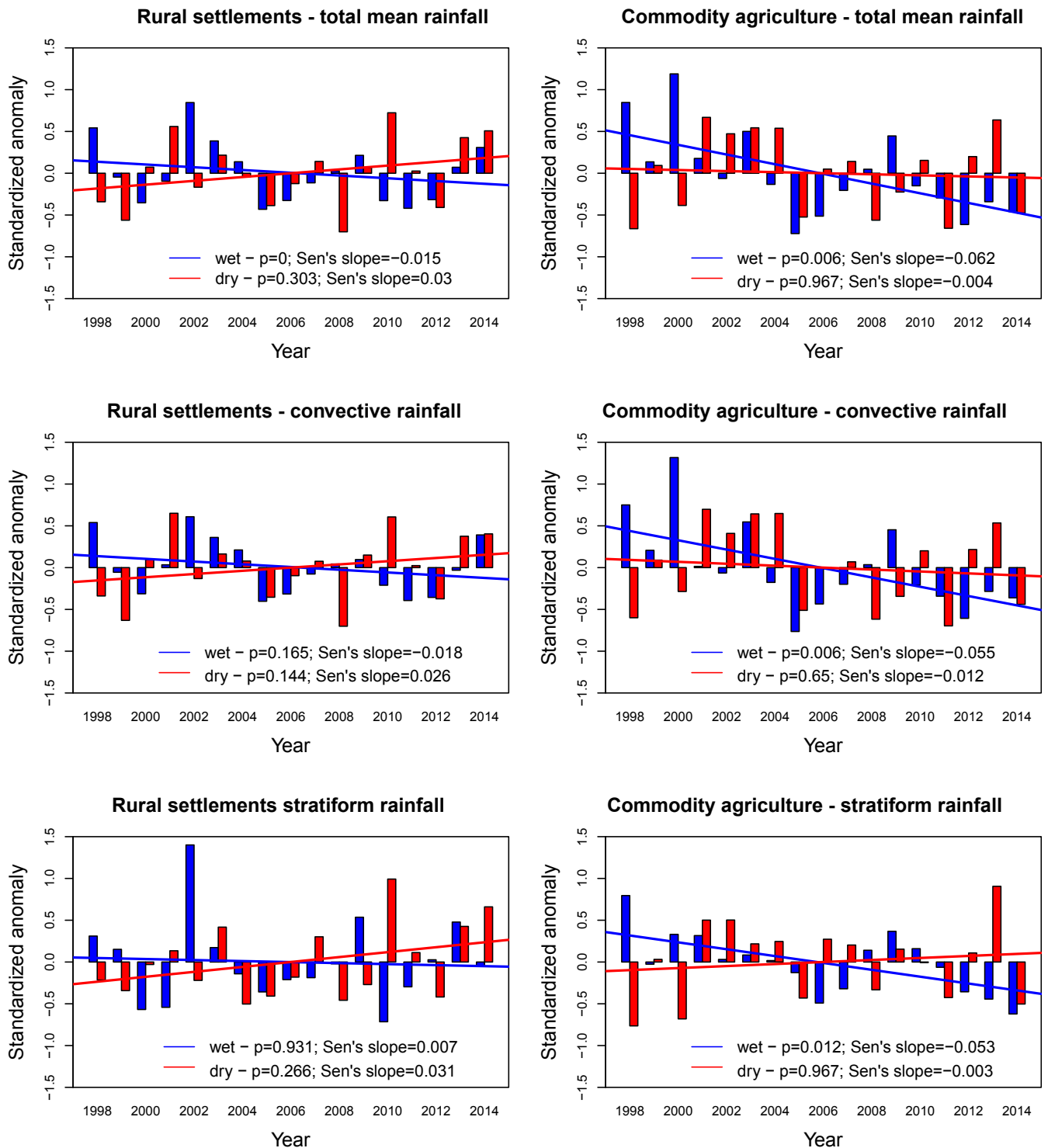


**Fig. 4.** Rainfall time series trends from 1998 to 2014. The wet period (blue) is represented by average rainfall values from October to March, while the dry period (red) is represented by the period between April and September. We define wet period as the period when average monthly rainfall in our study areas was above  $200 \text{ mm mo}^{-1}$ .

low as 75% between January and May in commodity agriculture areas (in comparison with 80% in rural settlements) (*SI Appendix, Fig. S7B*).

## Discussion

Our results demonstrate that taking into account the complex combination of matrix shape, land use, and land management is

key to understanding the climate impacts caused by deforestation in the Amazon forest. We provided evidence that regions with similar history of total forest loss can have quantitatively distinguishable spatial patterns depending on the original causes of deforestation, leading to different climate impacts.

We report a significant decline in wet season rainfall volumes in areas dominated by large-scale commodity agriculture. The

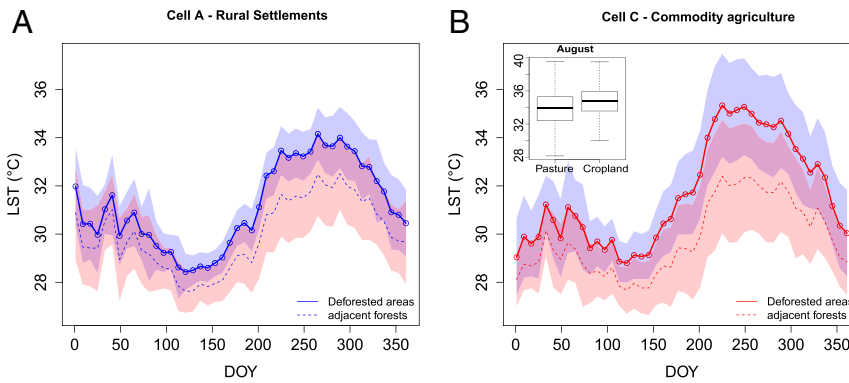


**Fig. 5.** Mean seasonal patterns of LST in (A) rural settlements and (B) commodity agriculture areas, with B, *Inset* showing results for dominant land use classes within the region. Average values were calculated using data from 2001 to 2018. Shaded areas represent means  $\pm$  SD.

same decline was not observed in an area where deforestation was mainly caused by rural settlements. Although the observed association between these two deforestation types and rainfall changes cannot prove a causal link, evidence from the causality can be deduced from the underlying physics driving the rainfall formation process. Previously published research collected evidence that changes in land surface properties can influence energy and moisture fluxes within the planetary boundary layer, as well as convective available potential energy, strongly affecting the development of cumulus convective rainfall (32). Modeling studies demonstrated that, as deforested areas increase and land cover becomes more uniform, convective lifting mechanisms lose force and local surface roughness starts to play a larger role in the regional climate dynamics (27). The decreasing rainfall in commodity agriculture areas could then be explained by the stronger reduction in LE in comparison with rural settlements, which leads to increasing aridity and weakening of convective lifting (33). This argument is confirmed by a stronger vapor pressure deficit (VPD) increase in the region dominated by commodity agriculture, in comparison with the rural settlement area (SI Appendix, Fig. S8). Within the commodity agriculture area, VPD in croplands was on average 5% higher than in pastures (and 10% higher than in pastures located in the rural settlement region).

Although the decrease in ET had a higher magnitude during the dry season, the effects of reduced ET on convective rainfall seemed more evident at the end of the rainy season (February to April). These findings are in line with previous studies indicating that ET reduction and surface warming lead to the drying of the atmospheric boundary layer, hindering cloud formation and

reducing rainfall (34). Studies have also demonstrated a large influence of forest loss on the ET patterns in the southern Amazon, reinforcing the role of forests in recycling precipitation by returning soil moisture back into the atmosphere (35).

The lower LE in commodity agriculture areas is likely explained by land management and crop phenology. Given the long growing season in the southern Amazon, crop production cycles are more complex than traditional cropping cycles found in temperate regions. In Mato Grosso State, for instance, the agricultural calendar can consist of multiple harvesting and seeding seasons (36). Soybean and maize seeding usually takes place between September and November, and harvesting is between January and May. This can be followed by another crop growing season (referred as “safrinha” in Portuguese), which occurs between February and September, usually consisting of maize or cotton.

The harvesting and seeding cycles typical for commodity crops lead to abrupt changes in the land surface properties, given the reduction of vegetation cover and exposure of bare land (18, 37, 38). This pattern is confirmed by the analysis of the EVI patterns over our sites. EVI is strongly related to photosynthetically active vegetation biomass (39, 40) and was shown to be efficient in monitoring agricultural production cycles (17), being a good indicator for crop mapping in southern Amazon (36). All these combined contribute to lower plant transpiration, reduced soil moisture, and changes in the surface energy balance. Such abrupt changes in the land surface are less likely to occur in rural settlement areas, given the different land use dynamics in these regions. Rural settlements are mostly characterized by pastures. Family farming and agroforestry also occur at smaller scales, which result

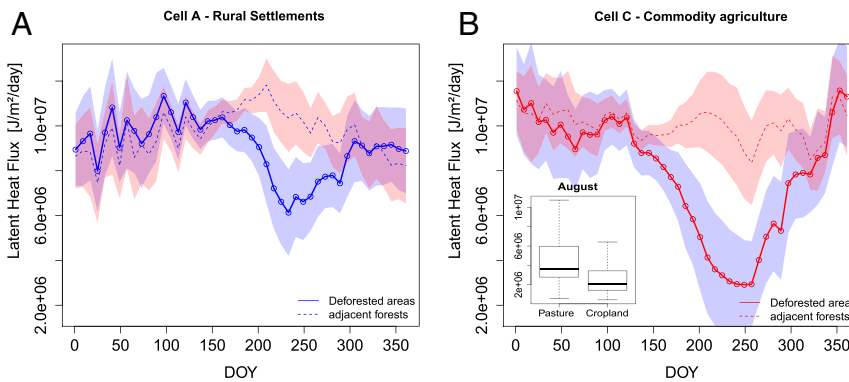


**Fig. 6.** Mean seasonal patterns of LE in (A) rural settlements and (B) commodity agriculture areas, with B, *Inset* showing results for dominant land use classes within the region. Average values were calculated using data from 2001 to 2018. Shaded areas represent means  $\pm$  SD.

in a more stable vegetation cover of the land surface, as the soil is not tilled or exposed during harvest.

When deforestation occurs, several factors contribute to changing the energy balance, which may lead either to the cooling or to the warming of the land surface. The resulting effects are mainly driven by two competing biophysical factors, ET and albedo (41). Forests typically absorb more shortwave radiation than sparser and lower vegetation (42, 43); consequently, the increase in surface albedo caused by forest loss often contributes to surface cooling. However, in tropical regions, nonradiative mechanisms (i.e., ET, surface roughness) are by far the dominant processes in energy budget changes caused by deforestation, leading to net warming (19, 24, 25, 41). Our results further refine these findings, demonstrating that land use and management patterns following deforestation are also critical for defining spatiotemporal patterns of surface energy balance. Overall, this is in line with previous studies indicating that forest to crop transitions have a more detrimental effect on ET, LE, and net surface radiation, when compared with forest to pasture transitions (5, 19).

However, the impacts of large-scale oscillations on the local climate trends observed in our study cannot be discarded, particularly the influence of atmospheric circulation patterns on the rainfall changes. Likewise, disentangling the effects of climate variability and land cover change on regional rainfall is challenging, as climate effects can mask deforestation-induced changes to the water budget (44). To improve our understanding of the ongoing climate changes in our study areas, we analyzed a time series of mean vertically integrated moisture divergence, which represents the horizontal rate of moisture flow (*SI Appendix, Fig. S9*). This parameter is positive for moisture that is spreading out and negative for the opposite, for moisture that is concentrating. Therefore, it indicates whether atmospheric motions act to decrease (for divergence) or increase (for convergence) the vertical integral of moisture, over the time period. Interestingly, our results indicate a decreasing trend of moisture divergence (increasing convergence) during the wet season, over all our study sites (*SI Appendix, Fig. S9*). These results are in line with previous research indicating that the Amazon basin has become substantially wetter since the 1990s, mainly due to increasing atmospheric water vapor import from the warming tropical Atlantic (45). This trend coincides with the onset of an increasing trend in tropical Atlantic sea surface temperatures (45). Thus, given the increasing moisture convergence in all study areas, our results provide evidence that the decreasing precipitation trend observed in commodity agriculture areas can be caused by local changes in land surface biophysical attributes.

The spatial (fish bone) patterns of deforestation caused by rural settlements have been known for decades. The higher shape index and core area of rural settlements demonstrate a greater overall landscape complexity in areas of rural settlement (46). The higher core area in rural settlements is initially counterintuitive, given that the region is characterized by smaller rural properties. The core area is defined as all cells that have no neighbor with a different class than themselves. Hence, our result in the rural settlement area is explained by a stronger connectivity between patches, which results in larger core areas, even though these areas may comprise several different rural properties.

Previous studies have gathered compelling evidence that the size of deforested areas is also important in defining the characteristics of local climatic changes. Small-scale forest loss was shown to increase regional cloudiness and precipitation frequency, due to enhanced mass and energy transfers between the land and the atmosphere (3, 26). On the other hand, this thermally triggered atmospheric circulation tends to get weaker as deforested area size increases, reducing rainfall rates (4, 27). Our results demonstrate that changes in land–atmosphere coupling not only are defined by the size of deforested areas but also, are

strongly dependent on land use and management patterns inside those areas.

These findings reinforce the argument that the impacts of modification and management of the land merit the same level of research and policy attention given to other anthropogenic contributions to climate change (47). We suggest that practices aiming to maximize vegetation cover should be further explored to mitigate changes in climate. These include, for instance, agroforestry or perennial crops cultivation (48). Agroforestry is a particularly attractive option, as it seeks to manage forest services and agriculture at the same time, improving soil fertility and increasing water availability while preserving vegetation cover and microclimate. Agroforestry systems are currently a very small element of the agricultural landscape in the Amazon, often at experimental scales or as a result of internationally funded initiatives (49).

Integrated crop–livestock systems are seen as a potential pathway to increase low productivity and sustainability of cattle production in the Amazon. The integrated soybean–cattle systems can have higher productivity than continuously grazed areas and hence, increased resilience under changing climate (50). In suitable areas, integrated crop–livestock systems can also be very profitable (51). However, both intercropping and rotation systems decrease vegetation cover in comparison with cattle grazing systems. Therefore, systems that also include trees (integrated crop–livestock–forestry systems) are recommended, considering our results.

On the other hand, traditional commodity agriculture in the southern Amazon is very productive, profitable, and technologically advanced. It is therefore farfetched to assume that alternative methods will replace the current system in the short term and at large scales. However, with increasing international awareness and consumers' preference for more sustainable products, alternative production methods will start to become more attractive. Actions led by the food industry and civil society organizations have been proven useful to guide in the direction of more sustainable practices. For instance, Brazil's soy moratorium, signed in 2006 by major soybean traders, limited the commercialization of soy grown on lands deforested after July 2006 in the Brazilian Amazon, having a positive impact on the reduction of deforestation rates while not affecting agricultural production (52, 53). Furthermore, there is increasing evidence that public policies, in combination with international trade treaties and protocols, have positive effects on sustainable land use and thus, the climate system (29).

Finally, restoration of legal forest reserves is another important pathway to mitigate changes in the regional climate. The recently created Rural Environmental Registry of private properties (CAR) will provide an unprecedented tool to monitor the compliance with the Brazilian forest code by linking a responsible landholder to land use on a particular farm (52, 53). This will thus allow the identification of suitable areas for forest restoration, as well as the creation of more sustainable supply chains.

## Materials and Methods

**Study Areas.** We selected four areas of  $\sim 110 \times 110$  km each ( $1^\circ \times 1^\circ$ ) (Fig. 1). As our aim was to compare areas dominated by commodity agriculture and rural settlements, we carried out a search for regions having similar total deforested area throughout the study period but distinct land use and spatial patterns. To select the suitable regions, the study areas had to meet the following criteria: have similar total deforested area; have similar temporal rates of deforestation within the analyzed time window; be big enough to provide a representative sampling and contain enough pixels from the remotely sensed data that were being evaluated (e.g., TRMM data at  $0.25^\circ$ ); be small enough to avoid confounding factors such as climate variability due to latitudinal differences or regional variability; have very distinct land use pattern (i.e., one needed to be dominated by rural settlements, and the other needed to be dominated by large-scale commodity

agriculture); and be far enough apart to avoid spatial autocorrelation of rainfall data.

To identify the regions meeting all the above criteria, we first divided the entire Amazon basin into a  $1^\circ \times 1^\circ$  grid. This cell size (i.e.,  $\sim 110 \times 110$  km) was considered consistent with the spatial resolution of all remote sensing datasets used in the study. The total deforested area inside each cell was calculated using land cover maps from MapBiomass project (<https://mapbiomas.org/en>) (*Land Use and Land Cover Data* has details). After identifying cells with similar total deforestation trajectories, we selected regions with distinct land use patterns based on 1) visual interpretation of spatial deforestation patterns, 2) size of rural properties according to Brazil's National Environmental Registry of Rural Properties, and 3) predominance of commodity crops, as identified by land use maps from MapBiomass project. The National Environmental Registry of Rural Properties is a mandatory and self-declaratory electronic registry for rural properties, in which owners must provide georeferenced data on the boundaries of the properties, as well as other information such as legal reserve areas and areas deforested.

We were also careful to select cells that were far enough apart to avoid spatial autocorrelation in the analysis of rainfall data. Rainfall patterns are defined not only by local land surface properties but also, by boundary conditions (e.g., synoptic conditions, atmospheric circulation). A study using more than 800 meteorological stations showed that the correlation coefficients of rainfall occurrence measured by stations distanced by less than 100 km were mostly above 0.8, decreasing to 0.4 or less for stations distanced by more than 500 km (54). The selected commodity agriculture and rural settlement regions are  $\sim 550$  km apart, thus avoiding major issues with spatial autocorrelation.

**Land Use and Land Cover Data.** Land use and land cover data were obtained from the MapBiomass project.\* We used Collection 4, released in August 2019, which covers the period from 1985 to 2018. This product offers land use and land cover maps at a 30-m spatial resolution. The maps are produced annually based on the classification of Landsat imagery mosaics. The mosaics are formed by a composition of the best-quality pixels in each set of images for a certain time period. The mosaics are then used to produce a map with land cover classes (forest, agriculture, pasture, urban area, water, etc.) using the random forest algorithm. All data are public and free for noncommercial use or general interest purposes. In this study, we reclassified the maps into four classes: forest, pasture, cropland, and mixed use. These four classes accounted for more than 99% of the total area in our study sites, during the entire study period. The forest class aggregated all the natural vegetation areas that did not suffer any conversion during the study period.

**Landscape Metrics.** To describe landscape patterns in the study areas affected by deforestation (marked as cells A and C in Fig. 1), we calculated landscape metrics for forest and nonforest land cover classes using FRAGSTATS 4.2 (46). Due to redundancy of the information provided by the various landscape metrics, we used the Pearson correlation test to discard highly correlated metrics ( $r \geq 0.80$ ). From the remaining eight metrics, we selected two that were less correlated with total forest loss (i.e., were more sensitive to landscape patterns/complexity and less sensitive to the class total area): mean shape index and mean core area (55). The shape index is the ratio between the perimeter of the patch and the hypothetical minimum perimeter of the patch. It equals zero if all patches have an identical shape index and increases, without limit, as the shapes of patches become more complex. The core area is defined by the cells that have only neighboring cells from the same class, and the mean core area equals the mean of core areas of all patches belonging to a certain class (46).

**EVI.** Vegetation cover over deforested areas was assessed using satellite-derived EVI, which is calculated based on the reflectance ( $\rho$ ) of red, blue, and near infrared (NIR) (40) following Eq. 1:

$$EVI = G \times \frac{(\rho_{NIR} - \rho_{Red})}{(\rho_{NIR} + C1 \times \rho_{Red} - C2 \times \rho_{Blue} + L)} \quad [1]$$

where  $\rho_{NIR}$  is the NIR reflectance factor,  $\rho_{Red}$  is the red reflectance factor, and

\*MapBiomass Project—Collection 4 of the Annual Land Use Land Cover Maps of Brazil was accessed through the link <https://mapbiomas.org>. MapBiomass Project is a multiinstitutional initiative to generate annual land use land cover maps based on automatic classification processes applied to satellite images. The complete project description can be found at <https://mapbiomas.org>.

$\rho_{Blue}$  is the blue reflectance factor; the coefficients adopted were  $L = 1$ ,  $C1 = 6$ ,  $C2 = 7.5$ , and  $G = 2.5$ .

The imagery was obtained from the Moderate Resolution Imaging Spectroradiometer (MODIS) Multi-Angle Implementation of Atmospheric Correction (MAIAC) product (MCD19A1) (56) at 1-km spatial resolution, which was downloaded from NASA's Level 1 and Atmosphere Archive and Distribution System (LAADS). We used MODIS Collection 6 Level 1B (calibrated and geometrically corrected) observations, which removed major sensor calibration degradation effects present in earlier collections. Observations collected between 2001 and 2018 were used in this study. MAIAC uses an adaptive time series analysis and processing of groups of pixels for advanced cloud detection, aerosol retrieval, and atmospheric correction. The data are corrected for sun-sensor-target geometry effects inherent in the image acquisition process. All the images are normalized to an apparent nadir view zenith angle ( $0^\circ$ ) and  $45^\circ$  of solar zenith angle using a bidirectional reflectance distribution function and Ross-Thick Li-Sparse model (56).

**Rainfall Data.** Rainfall data were obtained from the TRMM satellite, which was launched in November 1997 (57) and shut down in 2015. The product used was the 3A25, which consists of monthly statistics of the PR measurements (58). We used the  $0.5^\circ \times 0.5^\circ$  resolution grid, with monthly mean values of surface rainfall rate, which are classified between stratiform and convective types. The rain-type classification in TRMM PR products is done using two methods: the vertical profile method (59) and the horizontal pattern method (60). The vertical profile method is largely based on the detection of the bright band (BB), which indicates a melting layer, where the solid particles melt and change into rain drops. In the case of stratiform rain, the BB appears as a strong signal of radar echo when the radar frequency is between 15 and 20 GHz (59). This dataset and other TRMM data can be obtained through NASA's EARTHDATA search portal (<https://search.earthdata.nasa.gov/search>).

**LST.** LST data were obtained from the MODIS. The product used was the MOD11C2 Version 6, which provides LST imagery in a  $0.05^\circ \times 0.05^\circ$  latitude/longitude grid. The LST values in the MOD11C2 imagery are provided as composites, with pixel values representing the average of clear-sky LST during an 8-d period (61). All 8-d composites from 2001 to 2018 were used in this study.

The LST represents the radiometric temperature related to the thermal infrared radiation emitted from the land surface observed by an instantaneous MODIS observation. In this study, we used the daytime LST, corresponding to measurements obtained around 10:30 AM (local solar time). The MODIS LST products have been validated over a broad range of representative conditions and extensively tested using comparisons with in situ values and radiance-based validation. The product uncertainties are well defined, with LST errors estimated to be lower than 1 K in most cases (62).

In land areas, MODIS LST is only calculated for pixels at clear-sky conditions at 95% confidence for regions below 2,000 m above sea level and 66% confidence for regions above 2,000 m above sea level (61). In our study, quality control was undertaken using the quality assurance (QA) layers provided with the MOD11C2 product. The QA layer was used to exclude pixels in which LST was not produced due to atmospheric interference or not processed due to poor quality. Pixels with average LST error higher than 1 K were also excluded.

LST is known to be strongly affected by land cover characteristics (63–65). Given the different spatial resolutions between the LST data and the land cover maps, we carried out an additional analysis using high-resolution LST to exclude the influence of pixel mixture on our results. For that, we used a Landsat 8-based LST product with 30-m spatial resolution (66) (*SI Appendix, Fig. S6*). This product was shown to have an overall root-mean-squared error (RMSE) of  $1.52^\circ\text{C}$ , based on a comparison against two independently produced reference datasets. All cloud-free scenes obtained in dry seasons from 2013 to 2018 were considered, resulting in the five suitable images. The results obtained using the 30-m Landsat 8 LST product concurred with the conclusions based on the MODIS data, showing that areas occupied by commodity agriculture present significantly higher LST in comparison with areas occupied by rural settlements (*SI Appendix, Fig. S6*).

**VPD.** VPD was assessed using a remote sensing approach proposed by Hashimoto et al. (67). This method uses linear models to predict VPD using saturated vapor pressure calculated from MODIS LST. The saturation vapor pressure was calculated as follows (67):



$$e^*(T) = 0.6107e^{(17.38T)/(239+T)}, \quad [2]$$

where  $e^*(T)$  is given in kilopascals and  $T$  is the LST estimated by the MODIS sensor at around 10:30 AM. VPD was then calculated using the following linear model (67):

$$VPD = 0.353e^*(T) + 0.154. \quad [3]$$

Hashimoto et al. (67) tested this model in Porto Velho in the Brazilian Amazon, reporting an RMSE of 0.35 and a mean absolute error of 0.27.

**LE, Evaporation, and Transpiration.** LE and ET 8-d composite data, produced at 500-m spatial resolution, were obtained from the MODIS MOD16A2 product (68). LE is an important component of Earth's surface energy budget. It describes flux of energy from the land surface to the atmosphere that is associated with evaporation and transpiration of water (i.e., ET). The MOD16 LE and ET are estimated by a modified Penman–Monteith ET method, which uses ground-based meteorological observations and remote sensing data from MODIS (e.g., leaf area index [LAI], albedo, and land cover). Compared with eddy flux measurement, MODIS ET was shown to have a mean absolute error of  $\sim 0.3 \text{ mm d}^{-1}$  (68). All 8-d composites from 2001 to 2018 were used in this study.

ET partition between physical evaporation ( $E$ ) and transpiration was assessed using the method proposed by Wei et al. (69). This approach presents an ET partitioning algorithm based on the relationships between LAI and  $T/(E + T)$  for different vegetation types. The partition was done as follows:

$$\frac{T}{E + T} = 0.66 \times LAI^{0.18} \text{ (croplands)}, \quad [4]$$

$$\frac{T}{E + T} = 0.69 \times LAI^{0.28} \text{ (pastures)}, \quad [5]$$

where LAI is obtained from MOD15A2H Collection 6, MODIS LAI product. This is an 8-d composite dataset at 500-m resolution.

**Statistical Analysis of Changes in the Climate Variables.** Temporal changes in rainfall patterns were analyzed using two approaches. First, we analyzed rainfall seasonal patterns in two periods: 1985 to 2005 represents a period marked by an intensification of forest loss in our study areas, while the percentage forest loss in both areas was still below 40%; in the second period between 2005 and 2014, forest loss continued at a lower rate, with the percentage forest loss being close to 50%. This assessment was done at monthly timescale and considering total rainfall, convective rainfall fraction, and stratiform rainfall fraction separately. Changes in the mean annual rainfall values between these two periods were assessed, and statistical significance was checked using a Welsch  $t$  test. Next, rainfall temporal trends

were assessed using a modified version of the M-K trend test (70). This modified version of the M-K trend test reduces the chances of false positives by accounting for serial correlation, often present in time series data due to subsequent observations. The magnitude of the trends was assessed using Sen's slope (71), which is less vulnerable to errors in comparison with least squares estimator of a regression coefficient  $\beta$ , as well as less sensitive to nonnormality of the parent distribution and outliers.

Changes in EVI, LST, LE, and ET associated with forest loss were assessed using an SFT substitution approach (30, 31). The basic assumption in the SFT is that spatial and temporal variations are equivalent (30). Hence, observations of LST, LE, and ET over deforested areas were compared with those obtained over adjacent forests (i.e., intact forests located inside the same  $1^\circ \times 1^\circ$  cell). Deforested areas were identified using the land cover maps. Only areas that were deforested during the entire period of the MODIS time series used in this study (2001 to 2018) were used in the analysis. Given the coarser spatial resolution of MODIS data (500 m for LE and ET,  $\sim 5 \text{ km}$  for LST) in comparison with the land cover data (30 m), the influence of pixel mixing on LST, LE, and ET retrievals was minimized by eliminating MODIS pixels with more than 10% forest cover. Our analysis did not require resampling or pixel aggregation to resize the climate data (i.e., rainfall, LST, ET, and LE). Each climatic variable was analyzed independently and therefore, using the original resolution.

The SFT substitution is broadly used to infer temporal changes in ecological and biophysical systems using contemporary spatial patterns (24, 30, 31, 72). This approach is considered an alternative to long-term assessments, particularly in situations when long time series observations are not available. This is the case of our study, given that the MODIS time series used in our analysis is available starting from the year 2001.

**Data Availability.** Remotely sensed measurements of LST, rainfall, LE, and EVI are stored at NASA's Level-1 and Atmosphere Archive and Distribution System (LAADS) Distributed Active Archive Center (DAAC) (<https://ladsweb.modaps.eosdis.nasa.gov/>). Land cover maps were obtained from Project MapBiomass - Collection 4 of Brazilian Land Cover & Use Map Series, through the link <https://mapbiomas.org/>.

**ACKNOWLEDGMENTS.** This research was funded by Academy of Finland Decisions 318252 and 319905. T.A.A. is funded by the Academy of Finland Decision 318645. M.S. acknowledges funding from the Ministry for Foreign Affairs of Finland decision HEL7MO453-72 and supported by the Board of Education of Finland. L.E.O.C.A. was supported by the São Paulo Research Foundation (FAPESP) Grant 2018/15001-6 and National Council for Scientific and Technological Development Grant 305054/2016-3. Y.M.d.M. is funded by the Royal Society under Newton International Fellowship Scheme Grant NF170036. We thank Dr. Matheus Nunes for his insightful comments on and suggestions for a previous version of this manuscript and two anonymous reviewers for their thoughtful comments and efforts toward improving our manuscript.

1. E. A. Davidson et al., The Amazon basin in transition. *Nature* **481**, 321–328 (2012).
2. INPE, *PRODES-Monitoramento do Desmatamento da Floresta Amazônica Brasileira por Satélite* (Instituto Nacional de Pesquisas Espaciais, São José dos Campos, Brazil, 2020).
3. F. J. F. Chagnon, Contemporary climate change in the Amazon. *Geophys. Res. Lett.* **32**, L13703 (2005).
4. D. V. Spracklen, S. R. Arnold, C. M. Taylor, Observations of increased tropical rainfall preceded by air passage over forests. *Nature* **489**, 282–285 (2012).
5. D. V. Silvério et al., Agricultural expansion dominates climate changes in southeastern Amazonia: The overlooked non-GHG forcing. *Environ. Res. Lett.* **10**, 104015 (2015).
6. E. E. Maeda et al., Dynamic modeling of forest conversion: Simulation of past and future scenarios of rural activities expansion in the fringes of the Xingu National Park, Brazilian Amazon. *Int. J. Appl. Earth Obs. Geoinf.* **13** (2011).
7. B. H. Millikan, Tropical deforestation, land degradation, and society: Lessons from Rondonia, Brazil. *Lat. Am. Perspect.* **19**, 45–72 (1992).
8. D. S. Alves, Space-time dynamics of deforestation in Brazilian Amazônia. *Int. J. Remote Sens.* **23**, 2903–2908 (2002).
9. A. P. D. Aguiar, G. Câmara, M. I. S. Escada, Spatial statistical analysis of land-use determinants in the Brazilian Amazonia: Exploring intra-regional heterogeneity. *Ecol. Modell.* **209**, 169–188 (2007).
10. H. P. Binswanger, Brazilian policies that encourage deforestation in the Amazon. *World Dev.* **19**, 821–829 (1991).
11. P. Moutinho, R. Guerra, C. Azevedo-Ramos, Achieving zero deforestation in the Brazilian Amazon: What is missing? *Elem. Sci. Anthr.* **4**, 000125 (2016).
12. F. J. B. O. de Filho, J. P. Metzger, Thresholds in landscape structure for three common deforestation patterns in the Brazilian Amazon. *Lands. Ecol.* **21**, 1061–1073 (2006).
13. A. Mayer, "Agribusiness and family farming in Brazil: Competing modes of agricultural production" in *Land Use Competition*, J. Niewöhner et al., Eds. (Springer International Publishing, 2016), pp. 279–293.
14. V. Zalles et al., Near doubling of Brazil's intensive row crop area since 2000. *Proc. Natl. Acad. Sci. U.S.A.* **116**, 428–435 (2019).
15. D. C. Morton et al., Cropland expansion changes deforestation dynamics in the southern Brazilian Amazon. *Proc. Natl. Acad. Sci. U.S.A.* **103**, 14637–14641 (2006).
16. P. G. Curtis, C. M. Slay, N. L. Harris, A. Tyukavina, M. C. Hansen, Classifying drivers of global forest loss. *Science* **361**, 1108–1111 (2018).
17. J. C. Brown, J. H. Kastens, A. C. Coutinho, D. de C. Victoria, C. R. Bishop, Classifying multiyear agricultural land use data from Mato Grosso using time-series MODIS vegetation index data. *Remote Sens. Environ.* **130**, 39–50 (2013).
18. G. Oliveira et al., Effects of land-cover changes on the partitioning of surface energy and water fluxes in Amazonia using high-resolution satellite imagery. *Ecohydrology* **12**, e2126 (2019).
19. A. Beltrán-Przekurat, R. A. Pielke Sr, J. L. Eastman, M. B. Coughenour, Modelling the effects of land-use/land-cover changes on the near-surface atmosphere in southern South America. *Int. J. Climatol.* **32**, 1206–1225 (2012).
20. J. Barlow et al., The future of hyperdiverse tropical ecosystems. *Nature* **559**, 517–526 (2018).
21. E. T. A. Mitchard, The tropical forest carbon cycle and climate change. *Nature* **559**, 527–534 (2018).
22. N. M. Haddad et al., Habitat fragmentation and its lasting impact on Earth's ecosystems. *Sci. Adv.* **1**, e1500052 (2015).
23. R. Alkama, A. Cescatti, Biophysical climate impacts of recent changes in global forest cover. *Science* **351**, 600–604 (2016).
24. G. Duveiller, J. Hooker, A. Cescatti, The mark of vegetation change on Earth's surface energy balance. *Nat. Commun.* **9**, 679 (2018).
25. T. A. Abera, J. Heiskanen, P. Pellikka, M. Rautiainen, E. E. Maeda, Clarifying the role of radiative mechanisms in the spatio-temporal changes of land surface temperature across the Horn of Africa. *Remote Sens. Environ.* **221**, 210–224 (2019).

26. J. Wang *et al.*, Impact of deforestation in the Amazon basin on cloud climatology. *Proc. Natl. Acad. Sci. U.S.A.* **106**, 3670–3674 (2009).
27. J. Khanna, D. Medvigy, S. Fueglistaler, R. Walko, Regional dry-season climate changes due to three decades of Amazonian deforestation. *Nat. Clim. Chang.* **7**, 200–204 (2017).
28. J. Khanna, D. Medvigy, Strong control of surface roughness variations on the simulated dry season regional atmospheric response to contemporary deforestation in Rondônia, Brazil. *J. Geophys. Res. Atmos.* **119**, 13,067–13,078 (2014).
29. R. Mahmood, R. A. Pielke, C. A. McAlpine, Climate-relevant land use and land cover change policies. *Bull. Am. Meteorol. Soc.* **97**, 195–202 (2016).
30. S. T. A. Pickett, "Space-for-time substitution as an alternative to long-term studies" in *Long-Term Studies in Ecology*, G. E. Likens, Ed. (Springer, New York, NY, 1989), pp. 110–135.
31. J. L. Blois, J. W. Williams, M. C. Fitzpatrick, S. T. Jackson, S. Ferrier, Space can substitute for time in predicting climate-change effects on biodiversity. *Proc. Natl. Acad. Sci. U.S.A.* **110**, 9374–9379 (2013).
32. R. A. Pielke, Influence of the spatial distribution of vegetation and soils on the prediction of cumulus Convective rainfall. *Rev. Geophys.* **39**, 151–177 (2001).
33. D. Ellison *et al.*, Trees, forests and water: Cool insights for a hot world. *Glob. Environ. Change* **43**, 51–61 (2017).
34. D. G. Miralles, P. Gentile, S. I. Senéviratne, A. J. Teuling, Land-atmospheric feedbacks during droughts and heatwaves: State of the science and current challenges. *Ann. N. Y. Acad. Sci.* **1436**, 19–35 (2019).
35. M. J. Lathuilière, M. S. Johnson, S. D. Donner, Water use by terrestrial ecosystems: Temporal variability in rainforest and agricultural contributions to evapotranspiration in Mato Grosso, Brazil. *Environ. Res. Lett.* **7**, 024024 (2012).
36. R. D. V. Epiphanyo, A. R. Formaggio, B. F. T. Rudorff, E. E. Maeda, A. J. B. Luiz, Estimating soybean crop areas using spectral-temporal surfaces derived from MODIS images in Mato Grosso, Brazil. *Pesqui. Agropecu. Bras.*, **45** (2010).
37. D. Carrer, G. Pique, M. Ferlicoq, X. Ceamanos, E. Ceschia, What is the potential of cropland albedo management in the fight against global warming? A case study based on the use of cover crops. *Environ. Res. Lett.* **13**, 044030 (2018).
38. P. J. de O. P. de Souza, E. J. P. da Rocha, A. Ribeiro, E. B. de Souza, Radiation balance in a soybean ecosystem in the Amazon. *Rev. Cienc. Agron.* **41**, 582–592 (2010).
39. E. E. Maeda, J. Heiskanen, L. E. O. C. Aragão, J. Rinne, Can MODIS EVI monitor ecosystem productivity in the Amazon rainforest? *Geophys. Res. Lett.* **41**, 7176–7183 (2014).
40. A. Huete *et al.*, Overview of the radiometric and biophysical performance of the MODIS vegetation indices. *Remote Sens. Environ.* **83**, 195–213 (2002).
41. Y. Li *et al.*, Local cooling and warming effects of forests based on satellite observations. *Nat. Commun.* **6**, 6603 (2015).
42. A. Henderson-Sellers, M. F. Wilson, Surface albedo data for climatic modeling. *Rev. Geophys.* **21**, 1743 (1983).
43. A. K. Betts, J. H. Ball, Albedo over the boreal forest. *J. Geophys. Res. Atmos.* **102**, 28901–28909 (1997).
44. P. K. Panday, M. T. Coe, M. N. Macedo, P. Lefebvre, A. D. de Castanho, Deforestation offsets water balance changes due to climate variability in the Xingu River in eastern Amazonia. *J. Hydrol. (Amst.)* **523**, 822–829 (2015).
45. M. Gloor *et al.*, Intensification of the Amazon hydrological cycle over the last two decades. *Geophys. Res. Lett.* **40**, 1729–1733 (2013).
46. K. McGarigal, S. Cushman, E. Ene, *FRAGSTATS v4: Spatial Pattern Analysis Program for Categorical and Continuous Maps* (University of Massachusetts, Amherst, 2012), <http://www.umass.edu/landeco/research/fragstats/fragstats.html>.
47. R. A. Pielke, R. Mahmood, C. McAlpine, Land's complex role in climate change. *Phys. Today* **69**, 40–46 (2016).
48. J. D. Glover *et al.*, Increased food and ecosystem security via perennial grains. *Science* **328**, 1638–1639 (2010).
49. R. Porro *et al.*, "Agroforestry in the Amazon region: A pathway for balancing conservation and development" in *Agroforestry—the Future of Global Land Use*, P. K. R. Nair, D. Garrity, Eds. (Springer Netherlands, 2012), pp. 391–428.
50. J. D. B. Gil *et al.*, Tradeoffs in the quest for climate smart agricultural intensification in Mato Grosso, Brazil. *Environ. Res. Lett.* **13**, 064025 (2018).
51. J. C. dos Reis *et al.*, Assessing the economic viability of integrated crop–livestock systems in Mato Grosso, Brazil. *Renew. Agric. Food Syst.*, 1–12 (2019).
52. H. K. Gibbs, *et al.*, Brazil's soy moratorium. *Science* **347**, 377–378 (2015).
53. I. Roitman *et al.*, Rural Environmental Registry: An innovative model for land-use and environmental policies. *Land Use Policy* **76**, 95–102 (2018).
54. M. F. Hutchinson, Stochastic space-time weather models from ground-based data. *Agric. For. Meteorol.* **73**, 237–264 (1995).
55. L. McGarigal, B. Marks, *FRAGSTATS manual: Spatial pattern analysis program for quantifying landscape structure* (US Forest Service, Portland, OR, 1995).
56. A. I. Lyapustin *et al.*, Multi-angle implementation of atmospheric correction for MODIS (MAIAC). 3. Atmospheric correction. *Remote Sens. Environ.* **127**, 385–393 (2012).
57. G. J. Huffman *et al.*, The TRMM multisatellite precipitation analysis (TMPA): Quasi-global, multiyear, combined-sensor precipitation estimates at fine scales. *J. Hydrometeorol.* **8**, 38–55 (2007).
58. T. Iguchi, T. Kozu, R. Meneghini, J. Awaka, K. Okamoto, Rain-profiling algorithm for the TRMM precipitation radar. *J. Appl. Meteorol.* **39**, 2038–2052 (2000).
59. J. Awaka, T. Iguchi, K. Okamoto, TRMM PR standard algorithm 2A23 and its performance on bright band detection. *J. Meteorol. Soc. Jpn.* **87A**, 31–52 (2009).
60. M. Steiner, R. A. Houze, S. E. Yuter, Climatological characterization of three-dimensional storm structure from operational radar and rain gauge data. *J. Appl. Meteorol.* **34**, 1978–2007 (1995).
61. Z. Wan, New refinements and validation of the collection-6 MODIS land-surface temperature/emissivity product. *Remote Sens. Environ.* **140**, 36–45 (2014).
62. S.-B. Duan *et al.*, Radiance-based validation of land surface temperature products derived from Collection 6 MODIS thermal infrared data. *Int. J. Appl. Earth Obs. Geoinf.* **70**, 84–92 (2018).
63. M. Jin, R. E. Dickinson, Land surface skin temperature climatology: Benefitting from the strengths of satellite observations. *Environ. Res. Lett.* **5**, 044004 (2010).
64. E. E. Maeda, P. Hurskainen, Spatiotemporal characterization of land surface temperature in Mount Kilimanjaro using satellite data. *Theor. Appl. Climatol.* **118**, 497–509 (2014).
65. T. A. Abera, J. Heiskanen, P. Pellikka, E. E. Maeda, Rainfall–vegetation interaction regulates temperature anomalies during extreme dry events in the Horn of Africa. *Glob. Planet. Change* **167**, 35–45 (2018).
66. D. Parastatidis, Z. Mitraka, N. Chrysoulakis, M. Abrams, Online global land surface temperature estimation from Landsat. *Remote Sens.* **9**, 1208 (2017).
67. H. Hashimoto *et al.*, Satellite-based estimation of surface vapor pressure deficits using MODIS land surface temperature data. *Remote Sens. Environ.* **112**, 142–155 (2008).
68. S. Running, Q. Mu, M. Zhao, A. Moreno, MODIS global terrestrial evapotranspiration (ET) product 500 m, Version 1.5. (National Aeronautics and Space Administration, 2017). [https://ladsweb.modaps.eosdis.nasa.gov/missions-and-measurements/modis/MOD16\\_ET\\_User-Guide\\_2017.pdf](https://ladsweb.modaps.eosdis.nasa.gov/missions-and-measurements/modis/MOD16_ET_User-Guide_2017.pdf).
69. Z. Wei *et al.*, Revisiting the contribution of transpiration to global terrestrial evapotranspiration. *Geophys. Res. Lett.* **44**, 2792–2801 (2017).
70. H. B. Mann, Nonparametric tests against trend. *Econometrica* **13**, 245–259 (1945).
71. P. K. Sen, Estimates of the regression coefficient based on Kendall's Tau. *J. Am. Stat. Assoc.* **63**, 1379–1389 (1968).
72. T. A. Abera, J. Heiskanen, P. K. E. Pellikka, H. Adhikari, E. E. Maeda, Climatic impacts of bushland to cropland conversion in Eastern Africa. *Sci. Total Environ.* **717**, 137255 (2020).